ADVANCED FUNCTIONAL MATERIALS
www.afm-journal.de

Hollow Molybdate Microspheres as Catalytic Hosts for Enhancing the Electrochemical Performance of Sulfur Cathode under High Sulfur Loading and Lean Electrolyte

Lu Wang, Guo-Ran Li, Sheng Liu, and Xue-Ping Gao**

Lithium–sulfur battery possesses a high energy density; however, its application is severely blocked by several bottlenecks, including the serious shuttling behavior and sluggish redox kinetics of sulfur cathode, especially under the condition of high sulfur loading and lean electrolyte. Herein, hollow molybdate ($CoMoO_4$, $NiMoO_4$, and $MnMoO_4$) microspheres are introduced as catalytic hosts to address these issues. The molybdates present a high intrinsic electrocatalytic activity for the conversion of soluble lithium polysulfides, and the unique hollow spherical structure could provide abundant sites and spatial confinement for electrocatalysis and inhibiting shuttling, respectively. Meanwhile, it is demonstrated that the unique adsorption of molybdates toward polysulfides exhibits a "volcano-type" feature with the catalytic performance following the Sabatier principle. The $NiMoO_4$ hollow microspheres with moderate adsorption show the highest electrocatalytic activity, which is favorable for enhancing the electrochemical performance of sulfur cathode. Especially, the S/$NiMoO_4$ composite could achieve a high areal capacity of 7.41 mAh cm^{-2} (906.2 mAh g^{-1}) under high sulfur loading (8.18 mg cm^{-2}) and low electrolyte/sulfur ratio (E/S, 4 µL mg^{-1}). This work offers a new perspective on searching accurate rules for selecting and designing effective host materials in the lithium–sulfur battery.

1. Introduction

The pursuit of high energy density has motivated unremitting efforts in the new secondary batteries.[1] Lithium–sulfur (Li–S) battery has been considered as one of the most competitive candidates due to the high theoretical gravimetric and volumetric energy densities (2500 Wh kg^{-1}, 2800 Wh L^{-1}).[2–4] Nevertheless, the practical application of Li–S battery has been greatly challenged by several intrinsic defects, such as the insulating nature of sulfur and Li_2S, the shuttle effect of the soluble intermediate lithium polysulfides (LiPS) and the sluggish redox kinetics of sulfur. Inevitably, these drawbacks result in the low utilization, unsatisfactory Coulombic efficiency and fast capacity decay of sulfur cathode, especially under the condition of high sulfur loading and lean electrolyte.

Loading sulfur on effective host materials is a feasible strategy to combat these above problems and enhance the electrochemical performance of sulfur cathode. Carbon nanomaterials could improve the conductivity and provide physical blocks to LiPS, thus have been extensively studied.[5–8] However, the nonpolar carbon nanomaterials provide a relatively weak binding toward the polar LiPS, leading to the eventual shuttling of LiPS and the consequent fast capacity fading.[9,10] Thus, the polar hosts, such as metal oxides,[11–13] metals sulfides,[14–16] metal nitrides,[17,18] have been studied to alleviate the shuttle effect due to the strong affinities with LiPS. Importantly, some polar metal compounds could largely accelerate the redox kinetics of sulfur cathode, demonstrating as the effective catalysts for the conversion of soluble LiPS. In the meantime, the adsorption of LiPS on polar hosts is considered as the critical step of electrocatalysis for promoting the utilization and cycling stability of sulfur cathode.[19,20] Besides, the mass and volume of the introduced hosts could be greatly reduced by using the host materials with high catalytic activity and high tap density, facilitating the realization of the high gravimetric/volumetric energy density of Li–S battery.[21–23] Numerous hosts have been investigated and exhibited different capabilities in accelerating the electrochemical redox of LiPS and retarding the shuttle effect. However, the relevant catalytic mechanism is still not very clear and the accurate models for material selections are still unavailable, which greatly limit the efficient design of high-activity catalysts for Li–S battery. Since the adsorption is a vital step that determines the activation of LiPS on the host surface, the adsorption energy is conventionally used as a descriptor for selecting host materials in publications.[21,24–26] In the common perception, the stronger adsorption strength of the host materials toward LiPS is more favorable for lifting the electrochemical performance of sulfur cathode. However, according to the Sabatier principle, too strong or too weak adsorptions both

Dr. L. Wang, Prof. G.-R. Li, Dr. S. Liu, Prof. X.-P. Gao
Institute of New Energy Material Chemistry
School of Materials Science and Engineering
Renewable Energy Conversion and Storage Center
Nankai University
Tianjin 300350, China
E-mail: shengliu@nankai.edu.cn; xpgao@nankai.edu.cn

The ORCID identification number(s) for the author(s) of this article can be found under https://doi.org/10.1002/adfm.202010693.

DOI: 10.1002/adfm.202010693

impede the redox transformation.[27] Therefore, the adsorption behavior of LiPS on the catalyst surface needs to be more carefully studied.

Molybdate oxides possess unique electronic structure, high electrocatalytic activity and selectivity, and are investigated as lithium storage materials,[28,29] catalysts for many systems, including fuel cells, Li–O_2 batteries, oxygen evolution, hydrolysis, and dehydrogenation reactions.[30–35] In this work, for the first time, a series of molybdate oxides ($MMoO_4$, M=Co, Ni, and Mn) are introduced as the promising catalytic hosts of sulfur for constructing high-performance sulfur cathode. By controllably optimizing, the hollow molybdate microspheres are synthesized, which could provide sufficient space for sulfur loading as well as certain spatial confinement to the soluble LiPS. In the meantime, the as-prepared molybdate hosts possess the similar structure and surface area, which is in favor of conducting a comparative study to deeply understand the electrocatalysis in Li–S system. It is demonstrated that the sulfur-based composites with various molybdates exhibit remarkable differences in redox kinetics during LiPS reduction and the resulting cycling performance. Especially, $NiMoO_4$ with the moderate adsorption toward LiPS presents the optimized performance on the utilization and cycling stability of sulfur active materials. The corresponding sulfur cathode with high sulfur loading of 8.18 mg cm^{-2} delivers a high areal capacity of 7.41 mAh cm^{-2} (906.2 mAh g^{-1}) at low electrolyte/sulfur ratio (E/S, 4 µL mg^{-1}). The experimental results and computational analysis reveal a "volcano-type" relationship between the adsorption energy and the catalytic performance for the molybdates, different from the common view that the stronger adsorption favors Li–S battery. This result provides a rational view of more sophisticated designing on effective host materials for Li–S battery.

2. Results and Discussion

The preparation process of the molybdates ($MMoO_4$, M=Co, Ni, and Mn) is illustrated in **Scheme 1** including the solvothermal treatment and low-temperature calcination. During the solvothermal treatment, the precursors undergo the inside-out Oswald ripening process[36] and the proposed reaction mechanism is presented in Figure S1 (Supporting Information). The solvothermal parameters have a great impact on the morphologies of the as-prepared molybdates. By optimizing the reaction time (10 h) and pH value (pH < 1), as suggested in Figures S1–S3 (Supporting Information), the uniformly yolk-shell/hollow microspheres of molybdate oxides can be prepared with a diameter of 2–5 µm (**Figure 1**a,c,e). These structures are expected to provide abundant sites for sulfur loading. The sulfur/molybdate composites are prepared by the simple melting-diffusion method, and the sulfur is expected to be captured within the void as well as the surface. Meanwhile, the microspheres are composed of densely packed nano-sized primary particles, which provides numerous micropores on the spheres and greatly maximizes the catalytic surface for LiPS redox. Transmission electron microscopy (TEM) images further reveal that $CoMoO_4$ (CMO) and $NiMoO_4$ (NMO) specifically show as yolk-shell spheres, whereas $MnMoO_4$ (MMO) has a hollow spherical morphology (Figure 1a,c,e). In addition, the size and morphology of the primary particles and the shell thickness of these three molybdate microspheres are slightly different. The high-resolution transmission electron microscopy (HRTEM) images (Figure 1b,d,f) display clear lattice fringes of each as-prepared molybdate oxide, which could be well assigned to the lattice planes of $CoMoO_4$ (PDF #21-0868), $NiMoO_4$ (PDF #86-0361), and $MnMoO_4$ (PDF #82-2166), respectively.

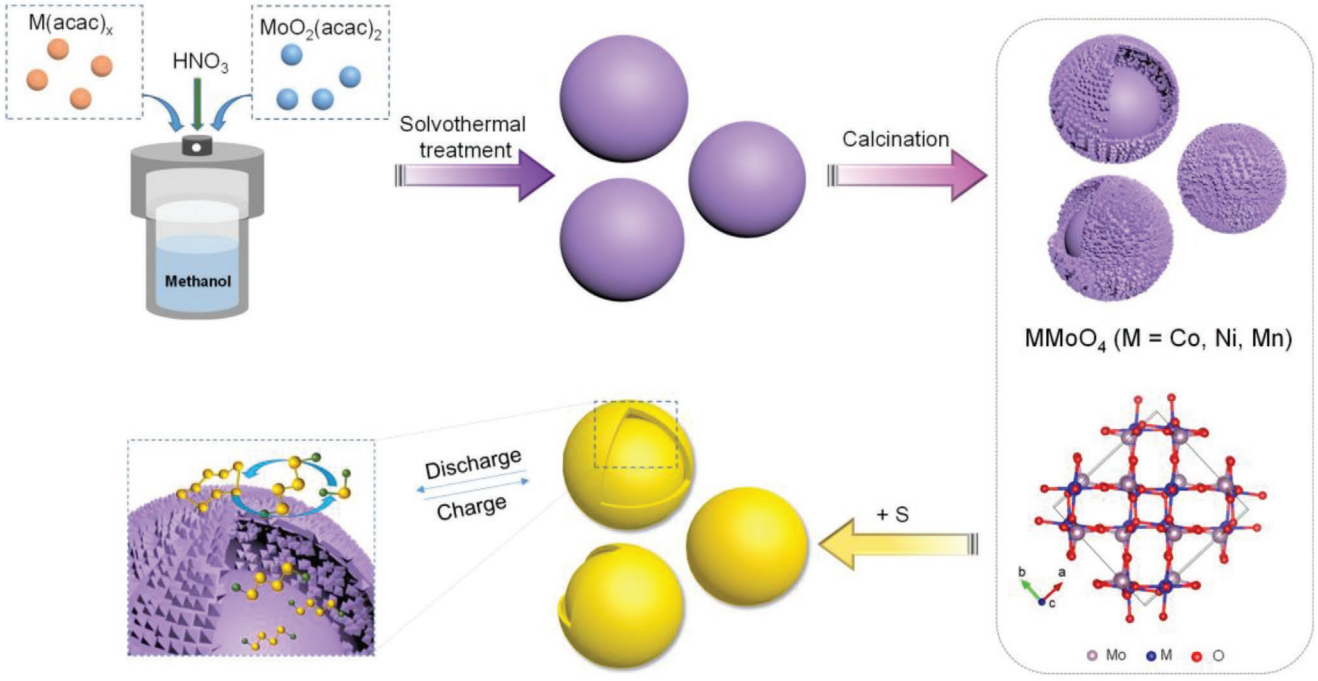

Scheme 1. Schematic illustration of the preparation process and structures of $MMoO_4$ and S/$MMoO_4$ (M=Co, Ni, and Mn).

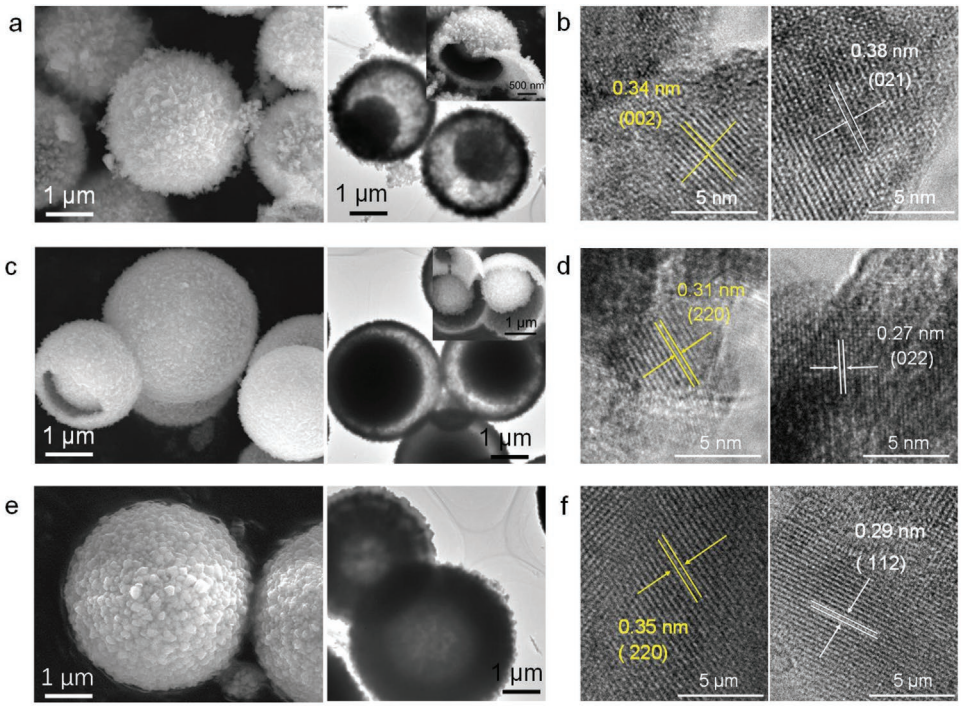

Figure 1. SEM and TEM/HRTEM images of a,b) CMO, c,d) NMO, and e,f) MMO.

The crystallographic structure of the molybdates is further confirmed by using X-ray diffraction (**Figure 2**a). Clearly, the obtained XRD patterns match well with the standard patterns of $MMoO_4$ (M=Co, Ni, and Mn) and are consistent with those reported in the literature,[33,36–38] demonstrating the as-prepared molybdates possess the same monoclinic phase. Note

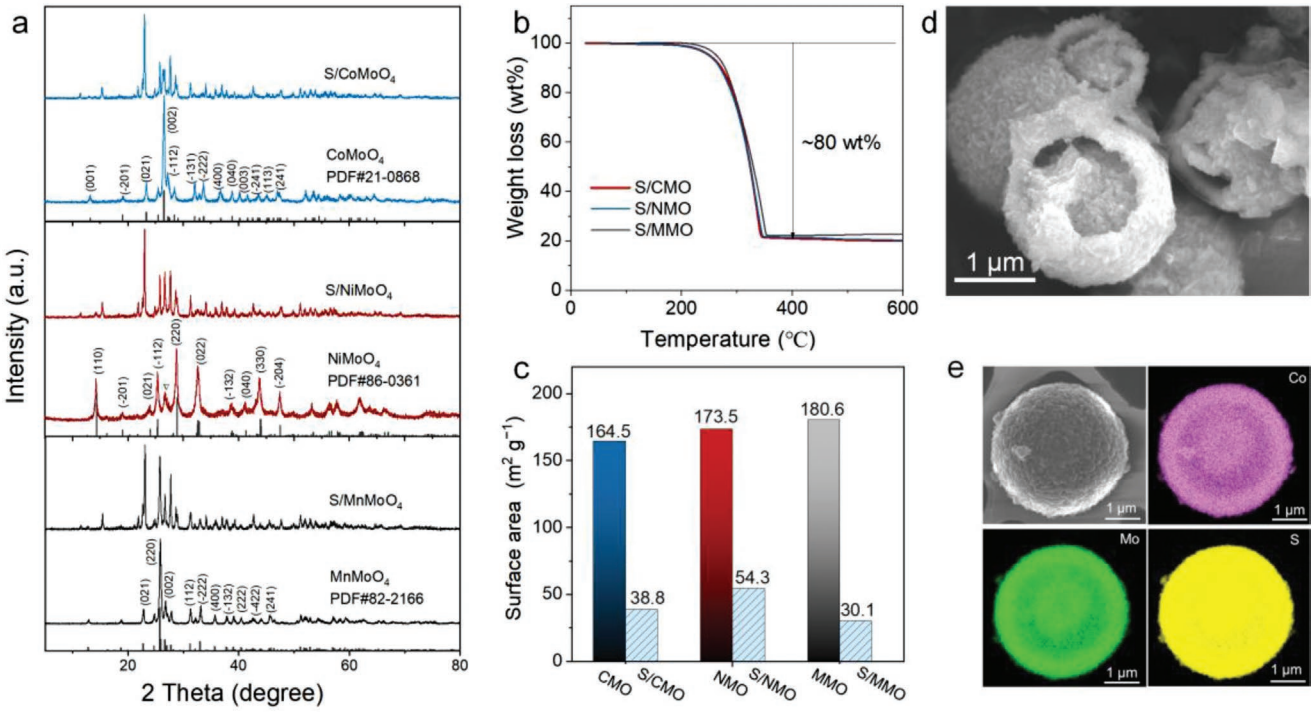

Figure 2. a) XRD patterns of $MMoO_4$ and $S/MMoO_4$ composites (M=Co, Ni, and Mn). b) TG curves of $S/MMoO_4$ composites. c) The surface area values of $MMoO_4$ before and after sulfur loading based on N_2 adsorption and desorption isotherms. d) SEM images of S/NMO. e) STEM and EDS elemental mapping of S/CMO.

that a peak at 26.6° in XRD patterns is not matched with the inserted standard pattern of α-$NiMoO_4$ (PDF #86-0361). This peak can be indexed to a trace amount of β-$NiMoO_4$ (PDF #12-0348), which also has the monoclinic crystal structure and is accompanied simultaneously with the α-$NiMoO_4$ under calcination.[37,38] In addition, XRD patterns of cobalt, nickel, manganese, and molybdate oxides are not detected. The textural properties of the molybdates can be determined by using N_2 adsorption–desorption isotherms. The as-prepared molybdates exhibit typical IV isotherms with Type H3 loops, suggesting the presence of the mesopores and slit-like pores[39] (Figure S4, Supporting Information). The emerged capillary condensation during adsorption at high pressure relates to the adsorbed behavior on mesopores, whereas the loops reflect the slit-like pores from the stacking of the molybdates particles. These three molybdate hosts possess similar surface areas of 163.5, 173.5, and 180.6 $m^2\ g^{-1}$ for CMO, NMO, and MMO, respectively (Figure 2c and Figure S4, Supporting Information). The large surface area of the as-prepared molybdate oxides could supply rich anchoring sites for LiPS, and the outer shells could provide the physical barrier to impede LiPS diffusion.

The sulfur contents in the corresponding S/$MMoO_4$ composites are approximate 80 wt%, as determined by the TG curves (Figure 2b). The characteristic diffraction peaks of molybdates and orthorhombic sulfur (PDF #08-0247) could be detected after sulfur loading (Figure 2a). Due to sulfur permeating, the surface area values of S/CMO, S/NMO and S/MMO drop to 39.8, 54.3, and 30.1 $m^2\ g^{-1}$, respectively. Meanwhile, pore volumes reduce from 0.354, 0.374, and 0.289 $cm^3\ g^{-1}$ to 0.042, 0.034, and 0.057 $cm^3\ g^{-1}$, respectively (Figure 2c, Figures S4 and S5, Supporting Information). SEM image of S/NMO indicates that sulfur is well coated on the shells of the microspheres, and partially encapsulated in the hollow sphere (Figure 2d). And the EDS elemental mapping images demonstrate sulfur could seep into the interior of the hollow spheres, while the skeleton structure of the molybdate oxides maintains stable (Figure 2e). The same structure together with the similar surface area of the host materials and the sulfur composites endows the feasibility to a comparative study on the intrinsic catalytic activity of the molybdate hosts. Besides, as the practical volumetric energy density of Li–S battery is still unsatisfactory, the tap density of the sulfur composite should be carefully considered.[11,40] Since CMO, NMO, and MMO possess inherent high theoretical densities (4.57, 4.95, and 4.18 g cm^{-3}, respectively) and sulfur is well integrated with the hollow spherical hosts, the obtained S/CMO, S/NMO, and S/MMO composites could achieve high tap densities of 1.61, 1.69, and 1.58 g cm^{-3}, respectively. These values are much higher than that of the conventional S/C (bp2000) composite (0.92 g cm^{-3}, Table S1, Supporting Information). The enhancement on the tap density of the sulfur composite provides the prerequisite for fabricating high-volumetric-capacity Li–S battery.

The electrochemical performance of the as-prepared S/$MMoO_4$ composites is evaluated with 2032-coin cells, and S/C (bp2000) composite is selected as the contrast. As shown in **Figure 3**a, the cycle performance of S/$MMoO_4$ composites is generally superior to the S/C composite, which means the introduction of the polar molybdates as the hosts is favorable for promoting the sulfur conversion. Notably, the sulfur composites based on different molybdates exhibit drastically different cycling performance. Specifically, S/NMO achieves the highest capacity of 1460.6 mAh g^{-1} at 0.05 C, followed by S/CMO (1356.3 mAh g^{-1}), S/MMO (1083.0 mAh g^{-1}), and S/C (1012.6 mAh g^{-1}). Note that the morphologies are slightly different, but the molybdates possess the similar surface areas. Since the catalytic feature is closely related to the exposed active sites, the electrochemical performance can be employed to investigate the difference in adsorption ability and catalytic activity of molybdates under the condition of the similar sulfur loading. The sulfur composites based on the molybdate hosts show a greater advantage in volumetric capacity than that based on carbon host, due to the higher tap density (Figure 3b, Figure S6 and Table S1, Supporting Information). Especially, the volumetric capacity of S/NMO could reach 1974.7 mAh $cm^{-3}_{\text{-composite}}$ at the current rate of 0.05 C, 2.65 times higher than that of the S/C composite (745.3 mAh $cm^{-3}_{\text{-composite}}$).

The electrochemical properties of S/$MMoO_4$ composites are further studied under high sulfur loading and low electrolyte usage, which are essential for achieving high energy density toward the practicality of Li–S battery. Under the high sulfur loading of ≈5.5 mg cm^{-2} and the low E/S of 4 µL mg^{-1}, S/NMO delivers higher initial capacity (890.5 mAh g^{-1}), as compared with those of S/CMO and S/MMO (Figure 3c,d). Moreover, the discharge capacities of S/NMO and S/CMO retain 609.2 and 538.3 mAh g^{-1} after 240 cycles at 0.1 C, respectively. However, the Li–S battery with the S/MMO cathode breaks down after 92 cycles with the capacity of 553.0 mAh g^{-1}, probably due to the weak adsorption ability and the resulting severe shuttle effect of LiPS under the high sulfur loading. Increasing the sulfur loading to 8.18 mg cm^{-2}, S/NMO could still deliver a high areal capacity of 7.41 mAh cm^{-2} (906.2 mAh g^{-1}) at 1 mA cm^{-2}, accompanied by a small polarization difference of 242 mV (Figure 3e,f). In addition, the areal capacity could stabilize at 6.47 mAh cm^{-2} (791.4 mAh g^{-1}) without obvious capacity decay after 120 cycles (Figure S7, Supporting Information). Comparing with S/NMO and S/CMO, S/MMO shows unsatisfactory cycling performance with larger polarization, lower capacity and shorter cycle life (Figure 3c–f). This difference could also be observed from the high-rate performance of these molybdates-based sulfur composites (Figure 3g,h). S/NMO delivers high capacities at the current rates of 2 C (734.7 mAh g^{-1}) and 5 C (571.5 mAh g^{-1}), exhibiting good high-rate capability. Besides, S/NMO shows excellent long-term cycling stability at 1 C with a low decay rate of 0.07% per cycle over 500 cycles. The above electrochemical results indicate NMO presents desirable features as an effective sulfur host, considering the high-rate capability, the high gravimetric/volumetric capacity and cycling stability under high sulfur loading and low electrolyte usage. The excellent electrochemical performance of S/NMO could be attributed to the unique structure and the effective catalysis of polar NMO host.

Despite these molybdate oxides possess the similar morphology, surface area, and sulfur loading, their impacts on improving the electrochemical performance are remarkably different. Thus, it can be speculated that this difference is closely related with the catalytic activities toward the conversion of sulfur species. In ether-based electrolyte, anchoring LiPS to restrain the shuttle effect and accelerating the redox

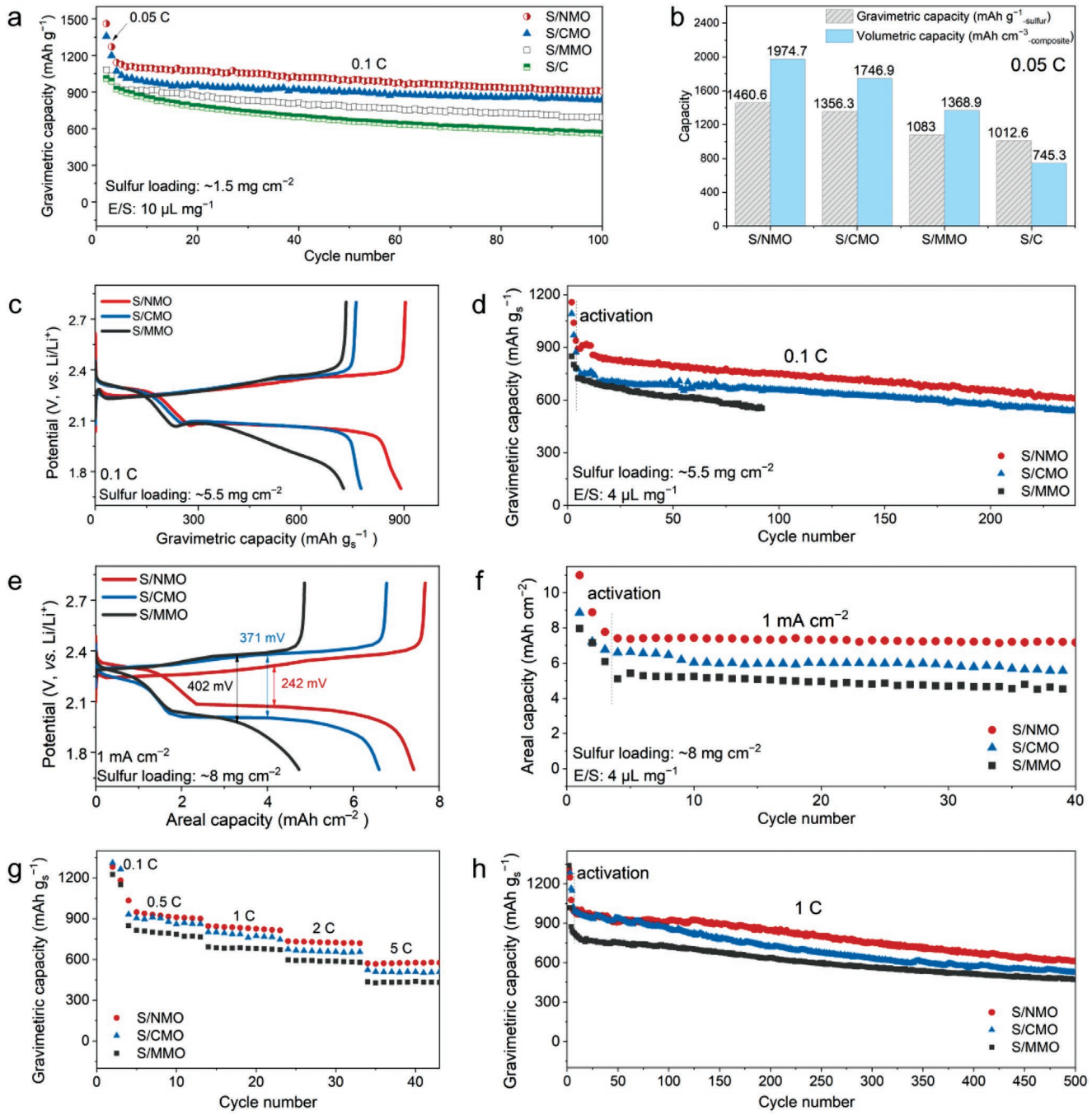

Figure 3. Electrochemical performance of S/$MMoO_4$ (M=Co, Ni, and Mn) and S/C composites. a) Cycling performance and b) volumetric capacities with the sulfur loading of ≈1.5 mg cm^{-2}. The initial charge/discharge curves and cycling performance of S/$MMoO_4$ composites with the high sulfur loading of c,d) ≈5.5, and e,f) ≈8 mg cm^{-2} at 0.1 C. g) The rate capabilities and h) long cycling performance of S/$MMoO_4$ composites.

kinetics from LiPS to Li_2S are critical to improve the sulfur utilization and maintain the cycling stability.[19,41] It is worthwhile to explore the catalytic conversion of LiPS on the as-prepared molybdate hosts. During the heterogeneous catalysis process, the adsorption of LiPS on the catalyst surface is an important step, which determines the activation of the LiPS and the subsequent electron transfer process. Therefore, the adsorption behavior of LiPS on various molybdates is carefully studied by the following measurements to investigate the mechanism of the catalytic reaction.

The entrapment ability of the molybdate hosts to LiPS is first examined with adsorption experiments and UV–vis measurements. The same amount of CMO, NMO, MMO, and the commercial carbon (bp2000) was separately added into Li_2S_6 solution (3 mmol L^{-1}). The photographs of the solutions after 4 h standing are shown in **Figure 4**a, and the corresponding

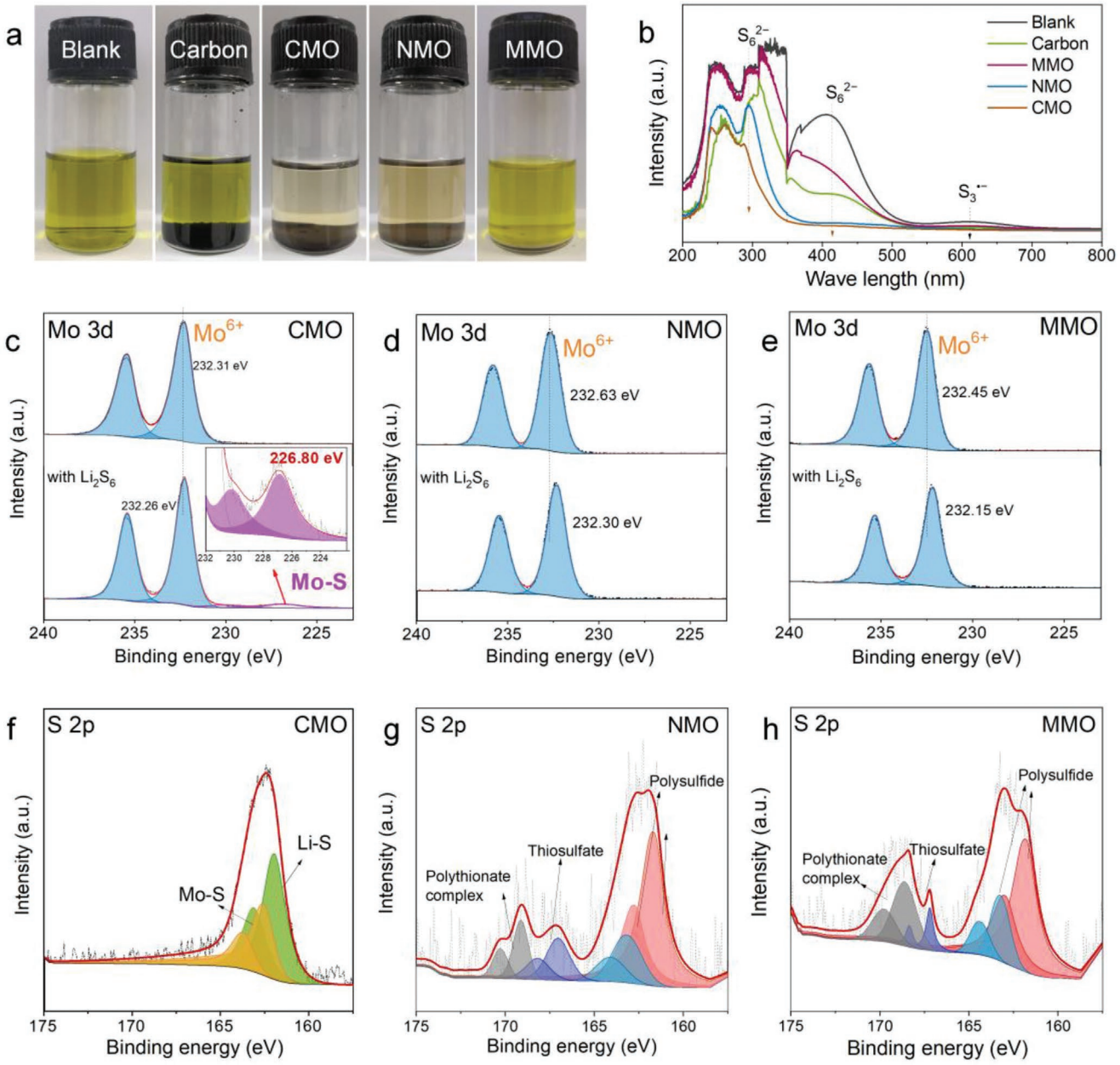

Figure 4. a) Visual discrimination and b) UV–vis spectra of the Li_2S_6 solutions (5 mL, 3 mmol L^{-1}) before and after adding 50 mg powers of CMO, NMO, MMO, and commercial carbon (bp2000) for 4 h. Mo 3d core spectra of pristine and Li_2S_6 treated c) CMO, d) NMO, and e) MMO. S 2p spectra of the sulfur species absorbed on the surface of f) CMO, g) NMO, and h) MMO.

UV–vis spectra are shown in Figure 4b. It could be observed that the solution immersed with CMO becomes completely colorless with the total disappearance of the characteristic peaks of Li_2S_6.[42] In addition, CMO caused the almost complete color fading within 5 min in the course of the experiment, suggesting a strong interaction with LiPS. NMO shows the second strong adsorption ability toward LiPS judging from the weak characteristic peaks of Li_2S_6. In contrast, the Li_2S_6 solutions immersed with MMO and the porous carbon show no significant changes in color and strong characteristic peak of Li_2S_6. It is worth noting that the light color of the solutions containing CMO and NMO is caused by the floating powders, as verified by the UV–vis spectra. Thus, the anchoring capability of the tested hosts toward LiPS could be easily concluded in the following sequence, CMO > NMO > carbon (bp2000) > MMO.

Generally, catalytic performance is closely related with the exposed active sites and the intrinsic catalytic activity.[41,43,44] As mentioned above, the as-prepared CMO, NMO and MMO possess similar surface area, corresponding to the similar number of active sites. Therefore, the difference in the adsorption and catalytic activity is mainly associated with the intrinsic electronic coupling between catalytic host and LiPS, which is affected by the surface chemistry and electronic structures of the molybdate oxides. To further probe the interaction pathway

between LiPS and $MMoO_4$ at the atomic level, X-ray photoelectron spectra (XPS) and density functional theory (DFT) calculations are performed.

The immersed CMO, NMO, and MMO powders are thoroughly dried for the XPS testing, and compared with the pristine samples. Mo in the pristine molybdate oxides resides in the oxidation state of Mo (VI) with a pair of Mo $3d_{5/2}$ (232.31–232.63 eV) and Mo $3d_{3/2}$ peaks,[45–47] with a slight difference in binding energy due to the discrepancies of surficial element compositions (Figure 4c–e). And Co, Ni, and Mn are all divalent (Figure S8, Supporting Information). After interacting with Li_2S_6, the binding energies of Co^{2+}, Ni^{2+}, and Mn^{2+} show certain negative shifts, indicating the formation of metal-sulfur bindings[48,49] (Figure S8, Supporting Information). However, the Mo 3d and S 2p core-level spectra of the immersed CMO show distinct differences with those of the immersed NMO and MMO. For Mo 3d spectrum of CMO, except the small shift to low binding energy of the Mo^{6+} peak, a new pair of $3d_{5/2}$ and $3d_{3/2}$ peaks arise at the very low binding energies (226.80 and 228.74 eV), corresponding to the newly formed Mo—S bond[50] (Figure 4c). The S $2p_{3/2}$ peak at 162.62 eV also confirms the existence of Mo—S bond[51], and the peak at 161.91 eV is assigned to Li—S bond[52] (Figure 4f). As for the immersed NMO and MMO, the Mo 3d peaks move ≈0.3 eV to lower binding energy and no new peaks appear (Figure 4d,e). On both the surface of NMO and MMO, thiosulfates/polythionate mediators at 167.0 and 168.8 eV could be detected, as well as the terminal and bridging sulfur of LiPS at 161.71 and 162.93 eV.[52] The thiosulfates/polythionate mediators could serve as the active sites for electron transfers.[52] The XPS spectra together with the adsorption experiments suggest the interaction mechanisms of these molybdate hosts toward LiPS are different. Specifically, CMO possesses strong interaction with Li_2S_6 mainly by forming Mo—S bond, whereas NMO and MMO could oxidize LiPS into thiosulfate/polythionate mediators to accelerate the conversion of LiPS. However, the interaction between MMO and LiPS is insufficient according to the weak color fading (Figure 4a).

To further reveal the detailed interaction and electronic structure regarding to the adsorption of Li_2S_n species on various molybdates, DFT calculations were carried out. The stable configurations of Li_2S_6 on various molybdate hosts are shown in **Figure 5**a–c. In addition, the specific interaction could be visualized taking advantage of the electron charge transfer analysis. In the case of CMO, the increase of charge occurs between S atom and Mo atom (pink part), denoting the formation of the strong Mo—S bond. In the meantime, charge loss appears along with the S—S bond inside Li_2S_6 (blue part), which may even induce the break of S—S bond (Figure 5a). With the similar analysis, the generation of Li—O bond and Ni—S bond for NMO, and Mn—S bond for MMO can be figured out (Figure 5b,c). The binding energy (E_b) shows the binding strength between LiPS and these molybdates, which are –2.83, –2.49, and –0.68 eV for the selected planes of CMO, NMO, and MMO, respectively. Obviously, the electrochemical coupling between CMO and Li_2S_6 is the strongest, which is in good agreement with the fast color fading in the adsorption experiment. For NMO, the binding strength is not as strong as CMO, but still remarkable. While binding energy for MMO is quite small, which could explain the weak anchoring effect of MMO observed in Figure 4a. The differences in electrochemical couplings and the consequent adsorption energy are the results of the different atomic structures of the host surfaces.

The different interactions between LiPS and host materials always lead to different catalytic activities and electrochemical behaviors. As the kinetics analysis often serves as a bridge between the macroscopic behavior of catalysts and the microscopic reaction pathways,[53] a series of electrochemical measurements including cyclic voltammetry (CV), linear sweep voltammetry (LSV) and electrochemical impedance spectroscopy (EIS) were conducted for interpreting the actual catalytic activity of molybdate oxides in the sulfur cathode.

The CV curves of the $S/MMoO_4$ (M=Ni, Co, Mn) all exhibit two pairs of reduction and oxidation peaks, corresponding to the stepwise redox behavior of sulfur in ether-based electrolyte (Figure 5d). Obviously, S/NMO shows better redox reversibility and faster kinetics with the reduced potential difference and the enhanced peak currents during the conversion process, as compared with S/CMO. As for S/MMO, both the reduction and the oxidation kinetics are relatively sluggish. CV tests at different scan rates from 0.1 to 0.5 mV s^{-1} are sequentially performed to investigate the ion diffusion behavior according to the Randles Sevcik equation, which is important to the sulfur conversion (Figure S9, Supporting Information).[54,55] As expected, the peak currents of peak R1, R2, and O2 all exhibit good linear relationships with the square root of scanning rates, indicating a diffusion-limited electrochemical behavior of sulfur cathodes (Figure 5e). The calculated slope values at cathodic (R1, R2) and anodic (O2) peaks of S/NMO composites are 185.87, 179.95, and 427.20 mA $V^{-0.5}$ $s^{0.5}$, respectively, which are the approximately maximum values among the three kinds of composites (Table S3, Supporting Information). And CMO also shows relatively high slopes, whereas the slopes for the peaks of S/MMO are much smaller. The above results illustrate that S/NMO and S/CMO possess better diffusion behaviors of LiPS for promoting the reaction kinetics.

As mentioned above, the full reduction of LiPS to Li_2S is crucial to obtain high capacity and cycling stability in Li–S battery. And the differences in the conversion rate of LiPS on these three molybdate hosts were elucidated by Tafel plots drawing from linear scanning voltammetry (LSV). The three-electrode cells are assembled with $MMoO_4$ electrodes as the working electrode, Li foil as the counter and reference electrodes, and Li_2S_6 catholyte as the electrolyte. The obtained LSV and Tafel plots (Figure 5f, g and Table S3, Supporting Information) demonstrate that the reduction of LiPS on NMO electrode appears higher onset potential (2.374 V) and exchange current density (0.84 mA cm^{-2}) in contrast with CMO electrode (2.366 V and 0.78 mA cm^{-2}) and MMO electrode (2.329 V and 0.67 mA cm^{-2}). Therefore, the charge transfer of LiPS on NMO host is more rapid compared with the CMO and MMO hosts. In addition, the participation capacity of Li_2S on different molybdates is compared through the potentiostatic discharge test.[56–58] The calculated Li_2S precipitation capacity on NMO electrode (306.4 mAh g^{-1}) is much higher than that on CMO (261.7 mAh g^{-1}) and MMO (230.2 mAh g^{-1}) electrodes (Figure S10, Supporting Information). It suggests that NMO could largely promote the conversion from LiPS to Li_2S, which is beneficial to increase the utilization of the sulfur active material.

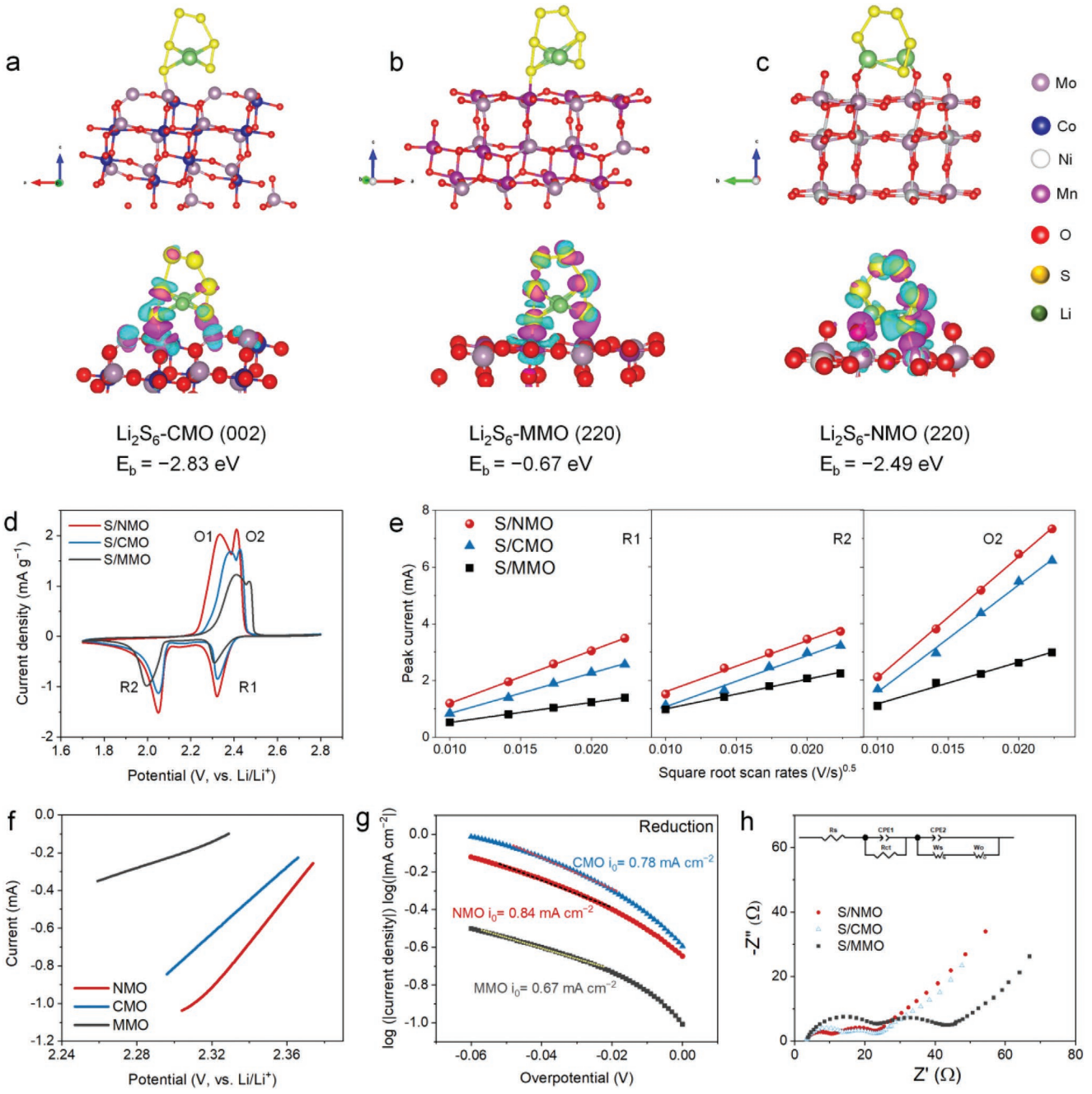

Figure 5. DFT calculation results of stable configurations and charge transfers when Li_2S_6 adsorbs on a) CMO, b) MMO, and c) NMO, where pink and blue represent the spatial regions gain and loss in charge, respectively. d) CV curves of S/NMO, S/CMO, and S/MMO. e) Plots of the peak currents versus the square root of scanning rates from CVs, for peak R1: S_8–Li_2S_4, peak R2: Li_2S_4–Li_2S, and peak O2: Li_2S_4–S_8, respectively. f) LSV and g) Tafel plots for the anodic process of CMO, NMO and MMO electrodes in Li_2S_6 electrolyte. h) EIS curves of S/NMO, S/CMO, and S/MMO composites discharged to the middle of the second plateau.

Furthermore, the reduction of LiPS needs to go through three steps of diffusion, adsorption and charge transfer, which could be well reflected on electrochemical impedance spectra (EIS). Thus, EIS of Li–S battery discharged to the middle of the second platform were tested to elucidate the conversion kinetics of LiPS on the molybdate hosts. As shown in Figure 5h, the obtained EIS plots consist of two semicircles and a slope line, which are related to the charge transfer, adsorption and diffusion processes of LiPS, respectively.[59] It is noted that S/NMO electrode shows the smallest diffusion impedance (W_o) and charge transfer resistance (R_{ct}) among these three cathodes, demonstrating the favorable diffusion and charge-transfer behavior of the soluble LiPS on NMO hosts. While the minimum adsorption impedance (W_s) appears on S/CMO cathode, illustrating the strong adsorption of LiPS on CMO hosts. Collectively, these above electrochemical measurements confirm that

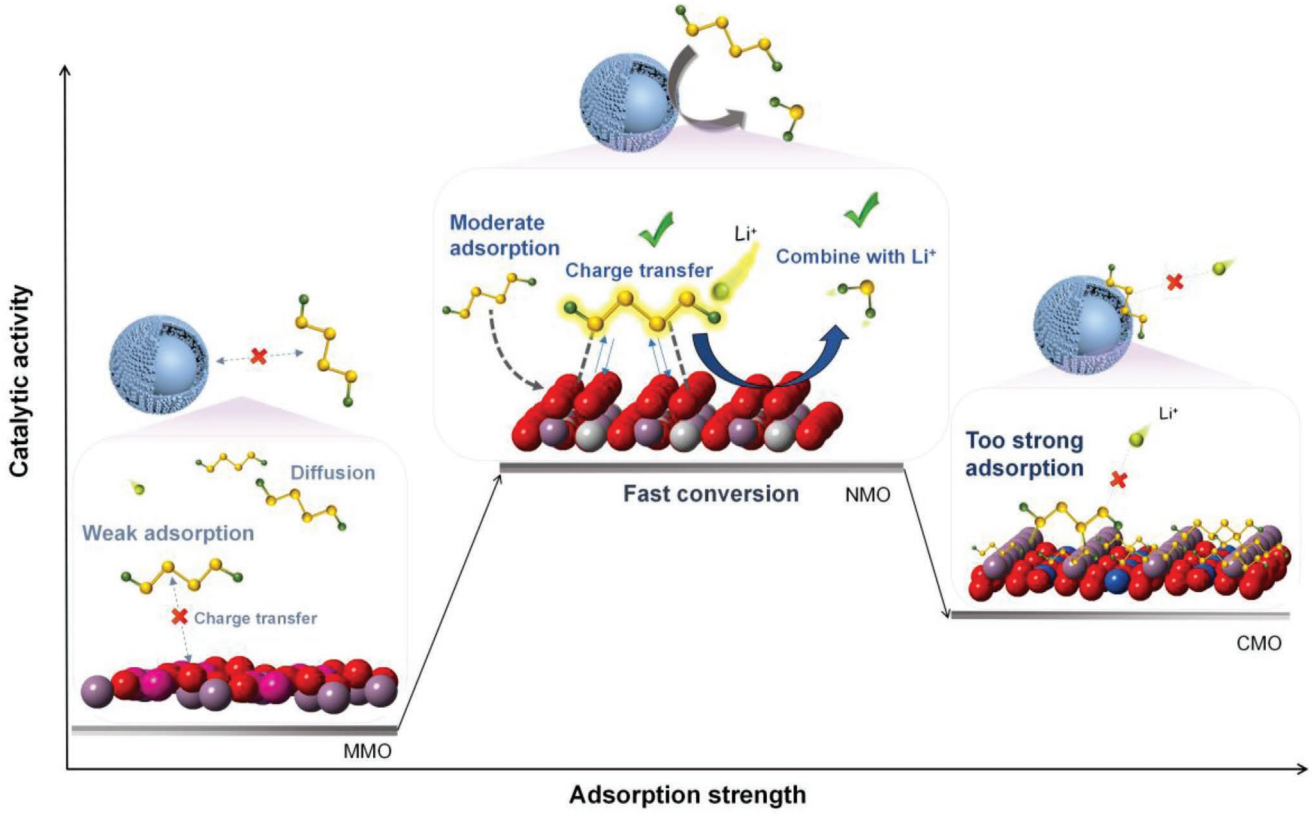

Figure 6. Representation showing the relationship between the adsorption strength and catalytic activity of various molybdate hosts.

NMO with the moderate adsorption possesses higher electrocatalytic activity for the redox kinetics of sulfur than that of CMO and MMO.

Usually, the strong chemical affinity to LiPS is a precondition for the subsequent fast-redox kinetics on the electrocatalysts.[21] However, some theoretical calculations in the previous reports also proved that the applied hosts with excessively strong adsorption toward LiPS could cause their decomposition.[9,60] In this study, it is demonstrated from the electrochemical measurements that CMO with the strongest adsorption energy is not the optimum host, whereas the NMO with the moderate adsorption shows the optimized electrochemical performance. These results illustrate that too strong adsorption of the catalytic host to LiPS may slow down the redox kinetics of sulfur cathode. Therefore, the catalytic activity of the as-prepared molybdate hosts shows volcano-like trends with the adsorption energy to LiPS following the Sabatier principle, that the adsorption energy should be just right, neither too strong nor too weak. This view can be demonstrated simply in **Figure 6**. It makes sense from the perspective that excessively strong binding of LiPS with the catalytic host would prevent its combination with the Li-ions and hamper subsequent electron transfer, leading to reduced reduction kinetics.[61] In addition, too strong adsorption would block the active sites for the consequent reactions.[53] And too weak adsorption would impair the adsorption process and the activation of the sulfur species, thus slow the latter conversion of LiPS, resulting in severe shuttling and the loss of the active materials. This interaction mechanism can be well illustrated by the comparative study on three molybdates, in which NMO exhibits the maximum lifting effect to the electrochemical kinetics and the performance of the sulfur cathode. Specifically, NMO could adsorb LiPS on the surface through the fairly strong polar-polar interaction, which could not only activate LiPS but also alleviate the shuttle effect. This process is more advantageous in the S/NMO cathode than in the S/MMO cathode, because NMO has stronger adsorption toward LiPS. Then, the activated LiPS on NMO could be easily reduced by combining with Li-ions. While the adsorption strength increases to a great extent for the CMO, the combination of LiPS with Li-ions will be hindered, thereby inhibiting the subsequent charge-transfer process. Therefore, the catalytic host materials should possess the moderate adsorption energy toward LiPS, and the surface electronic states of hosts are extremely crucial for the catalytic reaction. Importantly, as the adsorption energy is usually used as the descriptor of the catalyst, this concept is helpful to modulate the interfacial interaction to rationally design effective catalysts for Li–S battery.

3. Conclusion

In this work, molybdate hollow microspheres are successfully prepared and adopted as the catalytic hosts for Li–S battery. The unique hollow-sphere structure and the intrinsic high catalytic activity endow $NiMoO_4$ as an effective sulfur host to facilitate the conversion of LiPS and realize the high

gravimetric/volumetric energy density of the sulfur cathode. In particular, under the high sulfur loading of 8.18 mg cm^{-2}, the corresponding S/$NiMoO_4$ composite delivers a high gravimetric capacity of 7.41 mAh cm^{-2} (906.2 mAh g^{-1}). In addition, due to the high tap density, the volumetric capacity of S/$NiMoO_4$ reaches 1974.7 mAh $cm^{-3}_{\text{-composite}}$, almost 2.65 times of S/C composite. Besides, by the comparative study on the adsorption behavior, redox kinetics, electrochemical performance, and DFT calculations, we find the moderate adsorption of the host toward soluble polysulfides is effective to accelerate the redox process and enhance the electrochemical performance of Li–S battery. This work offers a thinking in effectively modulating the catalytic surfaces and designing high-efficiency catalytic hosts for Li–S battery.

4. Experimental Section

Preparation of S/$MMoO_4$ (M=Co, Ni, and Mn) Composites: $MMoO_4$ (M=Co, Ni, and Mn) were prepared by a solvothermal and sintering process, which is similar to the previous report.[36] In a typical synthesis of CMO, 1 mmol cobalt(III) acetylacetonate ($Co(acac)_3$, 99.9%, Alfa aesar) and 1 mmol $MoO_2(acac)_2$ (99.9%, Adamas) were dissolved in 100 mL methanol (99.9%, Acros Organics). Then HNO_3 (20 mL, 4 mol L^{-1}) was added into the above solution and stirred overnight. The obtained solution was then transferred into a Teflon-sealed autoclave (pressure resistance > 6 MPa), and heated at 200 °C for 10 h. The obtained precipitation was collected and washed with deionized water and ethanol, respectively. The recovered solid products were then heated at 450 °C for 3 h in the air to obtain the CMO, NMO and MMO were prepared with the same method by replacing $Co(acac)_3$ with $Ni(acac)_2$, $Mn(acac)_3$. The S/$MMoO_4$ composites were prepared with the simple melting–diffusion method by heating the mixture of sulfur and $MMoO_4$ at 155 °C for 12 h. The composites were fully ground and sifted before usage. The commercial carbon bp2000 was taken as the contrast host. And S/C (bp2000) composite was prepared with the same melting-diffusion method.

Materials Characterization: The morphology of the samples was characterized with SEM (JEOL, JSM-7800F). The crystal structure of $MMoO_4$ and S/$MMoO_4$ (M=Co, Ni, and Mn) composites was measured with XRD (Rigaku mini Flex II). TEM was performed on JEM-2100. N_2 adsorption-desorption isotherms were performed on JW-BK112 system with the Brunauer–Emmett–Teller (BET) model to test the specific surface areas of MMO and S/MMO composites. Thermogravimetric analysis (TG) was conducted on TGA/DSC 1 (Mettler-Toledo) to determine the sulfur content in the sulfur composites. The UV–vis adsorption spectrophotometry was conducted on Varian Cary 100 Conc UV–vis adsorption analyzer. And the X-ray photoelectron spectra were measured to acquire the chemical states of the samples in the adsorption experiment using Escalab 250Xi (Thermo Fisher Scientific). The tap density was measured with the following method. The mass of a dry measuring cylinder (m_1) was firstly weighed, then a certain amount of solid sample was added, followed by plugging the measuring cylinder and vibrating vertically for 3000 times. The volume of the sample after tapping (V) and the mass of the cylinder with the sample (m_2) were recorded. The tap density (ρ, g cm^{-3}) was calculated according to the formula: $\rho = (m_2 - m_1)/V$.

Adsorption and Nucleation Tests of Polysulfides: Li_2S_6 solution (3 mmol L^{-1}) was obtained by mixing Li_2S and S (1:5 in mole ratio) in 1,3-dioxolane/dimethyl ether (DOL/DME, 1:1 in volume) and heating at 60 °C for 48 h under stirring. Then 50 mg host material (molybdate or bp2000 carbon) was separately added into the as-prepared Li_2S_6 solution (5 mL). After immersion for 4 h, the UV–vis adsorption spectra of the liquid supernatants were tested. The residual solids were dried overnight for the XPS test.

The nucleation of Li_2S was tested on the CMO, NMO, and MMO electrodes, where the host material loading was 0.46 mg cm^{-2}. The Li_2S_8 catholyte (1.5 mol L^{-1}) was prepared by dissolving LiTFSI (1 mol L^{-1}), $LiNO_3$ (0.2 mol L^{-1}), Li_2S and S into the tetraglyme, and stirring at 60 °C for 48 h. Li foil (14 mm) was chosen as the counter electrode. During the assembly process of the CR2032 coin cell, 20 µL normal electrolyte was firstly dropped in the anode side, then 6 µL Li_2S_8 catholyte and 10 µL normal electrolyte was added in the cathode side. The assembled cells were first discharged galvanostatically to the start of the second platform at 0.03 C before the precipitation test of Li_2S, followed by the potentiostatically discharging at 2.06 V for 15 000 s.

Computational Methods: The modeling simulations were carried out with projector-augmented wave (PAW)[62] method as implemented in Vienna Ab-initio Simulation Package.[63] The generalized-gradient-approximation (GGA) as implemented by the Perdew–Burke–Ernzerhof (PBE) parameterization scheme was adopted to optimize the structures.[64] To simulate the adsorption on the surface of $MMoO_4$, a slab containing 72 atoms was constructed and a vacuum layer of 15 Å was built to prevent interactions between the two repeated layers. For all surface calculations, the bottom 24 atoms were kept frozen and the other atoms were allowed to relax. The Brillouin zone was sampled with 3 × 3 × 1 k-points of a Monkhorst-Pack grid[65] and the energy cutoff of 500 eV was adopted. The structure optimization was performed until the Hellmann–Feynman force on each atom was smaller than 0.02 eV $Å^{-1}$. The convergence of the total energy was considered to be achieved between subsequent iterations with energy difference less than 1×10^{-5} eV. The adsorption energy was calculated as $E_{ad} = E_{tot} - E_{Li2S6} - E_{MMoO4}$. In the equation, E_{tot} was the total energy of the adsorption Li_2S_6 and the $MMoO_4$ substrate, E_{Li2S6} and E_{MMoO4} were the energies of the Li_2S_6 and the $MMoO_4$ substrate, respectively.

Electrochemical Measurements: The cathodes were prepared by casting *N*-methyl pyrrolidone (NMP) slurry containing 70 wt% active material, 20 wt% conductive agent super P and 10 wt% binding agent polyvinylidene fluoride (PVdF) on carbon paper (TGP-H-060). The electrolyte was 1.0 M lithium bis(trifluoromethanesulphony)imide (LiTFSI) and 0.4 M $LiNO_3$ dissolved in the mixture of DOL and DME (1:1 ratio by volume). The cycling performance was tested using 2032-type coin cells between 1.7 and 2.8 V (versus Li/Li^+) at different rates (1 C = 1675 mA g^{-1}) on LANHE-CT2001A. The gravimetric capacities were calculated based on sulfur, and the volumetric capacities were calculated based on sulfur composite. Cyclic voltammetry measurements were performed on LK2005A workstation. EIS data were collected on IM6e electrochemical workstation (Zahner, Germany) in the range of 10 mHz–100 kHz. Linear sweep voltammetry (LSV) was carried out in a three-electrode cell, with $MMoO_4$ or bp2000 electrode as the working electrode, Li foil as the counter and the reference electrode, and 10 mmol L^{-1} Li_2S_6 in 5 mL normal electrolyte as the electrolyte.

Supporting Information

Supporting Information is available from the Wiley Online Library or from the author.

Acknowledgements

Financial supports from National Natural Science Foundation (21935006, 22075151) and Fundamental Research Funds for the Central Universities of China are gratefully acknowledged.

Conflict of Interest

The authors declare no conflict of interest.

Data Availability Statement

Data sharing is not applicable to this article as no new data were created or analyzed in this study.

Keywords

adsorption, electrocatalysis, lithium–sulfur batteries, molybdates, sulfur cathodes

Received: December 12, 2020
Revised: January 25, 2021
Published online:

[1] Z. W. Seh, Y. Sun, Q. Zhang, Y. Cui, *Chem. Soc. Rev.* **2016**, *45*, 5605.
[2] X. P. Gao, H. X. Yang, *Energy Environ. Sci.* **2010**, *3*, 174.
[3] X. L. Ji, L. F. Nazar, *J. Mater. Chem.* **2010**, *20*, 9821.
[4] J. W. Choi, D. Aurbach, *Nat. Rev. Mater.* **2016**, *1*, 1.
[5] M. Yan, H. Chen, Y. Yu, H. Zhao, C. F. Li, Z. Y. Hu, P. Wu, L. Chen, H. Wang, D. Peng, H. Gao, T. Hasan, Y. Li, B. L. Su, *Adv. Energy Mater.* **2018**, *8*, 1801066.
[6] Z. Zhang, L. L. Kong, S. Liu, G. R. Li, X. P. Gao, *Adv. Energy Mater.* **2017**, *7*, 1602543.
[7] Z. Y. Wang, Y. F. Dong, H. J. Li, Z. B. Zhao, H. B. Wu, C. Hao, S. H. Liu, J. S. Qiu, X. W. Lou, *Nat. Commun.* **2014**, *5*, 5002.
[8] Z. L. Li, Z. B. Xiao, S. Q. Wang, Z. B. Cheng, P. Y. Li, R. H. Wang, *Adv. Funct. Mater.* **2019**, *29*, 1902322.
[9] Q. Zhang, Y. Wang, Z. W. Seh, Z. Fu, R. Zhang, Y. Cui, *Nano Lett.* **2015**, *15*, 3780.
[10] Q. Pang, C. Y. Kwok, D. Kundu, X. Liang, L. F. Nazar, *Joule* **2019**, *3*, 136.
[11] L. Wang, Y. H. Song, B. H. Zhang, Y. T. Liu, Z. Y. Wang, G. R. Li, S. Liu, X. P. Gao, *ACS Appl. Mater. Interfaces* **2020**, *12*, 5909.
[12] L. Wang, Z. Y. Wang, J. F. Wu, G. R. Li, S. Liu, X. P. Gao, *Nano Energy* **2020**, *77*, 105173.
[13] Y. T. Liu, D. D. Han, L. Wang, G. R. Li, S. Liu, X. P. Gao, *Adv. Energy Mater.* **2019**, *9*, 1803477.
[14] K. Xi, D. Q. He, C. Harris, Y. K. Wang, C. Lai, H. L. Li, P. R. Coxon, S. J. Ding, C. Wang, R. V. Kumar, *Adv. Sci.* **2019**, *6*, 1800815.
[15] J. Xu, W. X. Zhang, H. B. Fan, F. L. Cheng, D. W. Su, G. X. Wang, *Nano Energy* **2018**, *51*, 73.
[16] H. T. Wang, Q. F. Zhang, H. B. Yao, Z. Liang, H. W. Lee, P. C. Hsu, G. Y. Zheng, Y. Cui, *Nano Lett.* **2014**, *14*, 7138.
[17] Z. M. Cui, C. X. Zu, W. D. Zhou, A. Manthiram, J. B. Goodenough, *Adv. Mater.* **2016**, *28*, 6926.
[18] X. X. Li, B. Gao, X. Huang, Z. J. Guo, Q. W. Li, X. M. Zhang, P. K. Chu, K. F. Huo, *ACS Appl. Mater. Interfaces* **2019**, *11*, 2961.
[19] K. Mahankali, S. Nagarajan, N. K. Thangavel, S. Rajendran, M. Yeddala, L. M. R. Arava, *Catalysts* **2020**, *10*, 1137.
[20] L. L. Peng, Z. Y. Wei, C. Z. Wan, J. Li, Z. Chen, D. Zhu, D. Baumann, H. T. Liu, C. S. Allen, X. Xu, A. I. Kirkland, I. Shakir, Z. Almutairi, S. Tolbert, B. Dunn, Y. Huang, P. Sautet, X. F. Duan, *Nat. Catal.* **2020**, *3*, 762.
[21] J. R. He, A. Bhargav, A. Manthiram, *Adv. Mater.* **2020**, *32*, 2004741.
[22] Z. Y. Wang, L. Wang, S. Liu, G. R. Li, X. P. Gao, *Adv. Funct. Mater.* **2019**, *29*, 1901051.
[23] Z. Zhang, D. H. Wu, Z. Zhou, G. R. Li, S. Liu, X. P. Gao, *Sci. China Mater.* **2019**, *62*, 74.
[24] Y. W. Wang, W. J. Qiu, E. Song, F. Gu, Z. H. Zheng, X. L. Zhao, Y. Q. Zhao, J. J. Liu, W. Q. Zhang, *Natl. Sci. Rev.* **2018**, *5*, 327.
[25] Y. C. Lu, H. A. Gasteiger, Y. Shao-Horn, *J. Am. Chem. Soc.* **2011**, *133*, 19048.
[26] Z. Q. Ye, Y. Jiang, J. Qian, W. L. Li, T. Feng, L. Li, F. Wu, R. J. Chen, *Nano Energy* **2019**, *64*, 103965.
[27] J. K. Nørskov, T. Bligaard, J. Rossmeisl, C. H. Christensen, *Nat. Chem.* **2009**, *1*, 37.
[28] C. T. Cherian, M. V. Reddy, S. C. Haur, B. V. Chowdari, *ACS Appl. Mater. Interfaces* **2013**, *5*, 918.
[29] J. S. Park, J. S. Cho, Y. C. Kang, *J. Power Sources* **2018**, *379*, 278.
[30] X. D. Yan, L. H. Tian, S. Atkins, Y. Liu, J. B. Murowchick, X. B. Chen, *ACS Sustainable Chem. Eng.* **2016**, *4*, 3743.
[31] Y. Tong, P. Z. Chen, M. X. Zhang, T. P. Zhou, L. D. Zhang, W. S. Chu, C. Z. Wu, Y. Xie, *ACS Catal.* **2017**, *8*, 1.
[32] C. Mazzocchia, C. Aboumrad, C. Diagne, E. Tempesti, J. M. Herrmann, G. Thomas, *Catal. Lett.* **1991**, *10*, 181.
[33] G. H. Lee, S. Lee, J. C. Kim, D. W. Kim, Y. Kang, D. W. Kim, *Adv. Energy Mater.* **2017**, *7*, 1601741.
[34] M. Q. Yu, L. X. Jiang, H. G. Yang, *Chem. Commun.* **2015**, *51*, 14361.
[35] J. Liao, D. Lu, G. Diao, X. Zhang, M. Zhao, H. Li, *ACS Sustainable Chem. Eng.* **2018**, *6*, 5843.
[36] G. S. Dong, H. Zhao, Y. M. Xu, X. F. Zhang, X. L. Cheng, S. Gao, L. H. Huo, *J. Alloys Compd.* **2019**, *785*, 563.
[37] S. K. Ray, B. Pant, M. Park, J. Hur, S. W. Lee, *Ceram. Int.* **2020**, *46*, 19022.
[38] B. Senthilkumar, K. V. Sankar, R. K. Selvan, M. Danielleb, M. Manickam, *RSC Adv.* **2013**, *3*, 352.
[39] M. Kruk, M. Jaroniec, *Chem. Mater.* **2001**, *13*, 3169.
[40] Y. T. Liu, S. Liu, G. R. Li, T. Y. Yan, X. P. Gao, *Adv. Sci.* **2020**, 1903693.
[41] Z. Zhang, D. Luo, G. R. Li, R. Gao, M. Li, S. Li, L. Zhao, H. Z. Dou, G. B. Wen, S. Sy, Y. F. Hu, J. D. Li, A. P. Yu, Z. W. Chen, *Matter* **2020**, *3*, 1.
[42] Q. L. Zou, Y. C. Lu, *J. Phys. Chem. Lett.* **2016**, *7*, 1518.
[43] Y. Jiao, Y. Zheng, K. Davey, S. Z. Qiao, *Nat. Energy* **2016**, *1*, 1.
[44] J. He, A. Manthiram, *Energy Storage Mater.* **2019**, *20*, 55.
[45] C. Choi, D. Y. Lee, J. B. Park, D. W. Kim, *ACS Sustainable Chem. Eng.* **2020**, *8*, 15134.
[46] R. Zhuang, S. Yao, X. Shen, T. Li, *J. Electroanal. Chem.* **2019**, *833*, 441.
[47] R. Zhuang, S. Yao, X. Shen, T. Li, *Int. J. Energy Res.* **2019**, *43*, 1111.
[48] Q. Pang, D. Kundu, M. Cuisinier, L. F. Nazar, *Nat. Commun.* **2014**, *5*, 4759.
[49] Y. Zhong, K. R. Yang, W. Liu, P. He, V. Batista, H. Wang, *J. Phys. Chem. C* **2017**, *121*, 14222.
[50] K. F. McCarty, J. W. Anderegg, G. L. Schrader, *J. Catal.* **1985**, *93*, 375.
[51] G. C. Stevens, T. Edmonds, *J. Catal.* **1975**, *37*, 544.
[52] X. Liang, C. Hart, Q. Pang, A. Garsuch, T. Weiss, L. F. Nazar, *Nat. Commun.* **2015**, *6*, 5682.
[53] Y. Mao, J. F. Chen, H. F. Wang, P. Hu, *Chin. J. Catal.* **2015**, *36*, 1596.
[54] X. Y. Tao, J. G. Wang, C. Liu, H. T. Wang, H. B. Yao, G. Y. Zheng, Z. W. Seh, Q. X. Cai, W. Y. Li, G. M. Zhou, C. X. Zu, Y. Cui, *Nat. Commun.* **2016**, *7*, 11203.
[55] G. M. Zhou, H. Z. Tian, Y. Jin, X. Y. Tao, B. F. Liu, R. F. Zhang, Z. W. Seh, D. Zhuo, Y. Y. Liu, J. Sun, J. Zhao, C. X. Zu, D. S. Wu, Q. F. Zhang, Y. Cui, *Proc. Natl. Acad. Sci. USA* **2017**, *114*, 840.
[56] C. Choi, J. B. Park, D. W. Kim, *J. Mater. Chem. A* **2020**, *8*, 25411.
[57] N. Wei, J. Cai, R. Wang, M. Wang, W. Lv, H. Ci, J. Sun, Z. Liu, *Nano Energy* **2019**, *66*, 104190.
[58] F. Y. Fan, W. C. Carter, Y. M. Chiang, *Adv. Mater.* **2015**, *27*, 5203.
[59] G. R. Li, J. Song, G. L. Pan, X. P. Gao, *Energy Environ. Sci.* **2011**, *4*, 1680.
[60] Y. K. Wang, R. Zhang, J. Chen, H. Wu, S. Lu, K. Wang, H. Li, C. J. Harris, K. Xi, R. V. Kumar, S. Ding, *Adv. Energy Mater.* **2019**, *9*, 1900953.
[61] G. K. P. Dathar, W. A. Shelton, Y. Xu, *J. Phys. Chem. Lett.* **2012**, *3*, 891.
[62] P. E. Blochl, *Phys. Rev. B* **1994**, *50*, 17953.
[63] G. Kresse, *Phys. Rev. B* **1996**, *54*, 11169.
[64] J. P. Perdew, K. Burke, M. Ernzerhof, *Phys. Rev. B* **1996**, *77*, 3865.
[65] H. J. Monkhorst, J. D. Pack, *Phys. Rev. B* **1976**, *13*, 5188.